“Synthesis and characterization of multiferroic AFe2O4-BiFeO3 (A=Co, Ni, Zn) nanocomposite thin films”

Major Research Project

Final Report Submitted to

University Grants Commission, New Delhi

by

Dr. Puneet Sharma

Associate Professor,

School of Physics and Materials Science

Thapar University, Patiala – 147004

June 2014

1. Introduction

Multiferroic composites

The broad and enthusiastic study towards multiferroic materials has been paid huge attention due to their potential applications in electronic devices [1-3]. To overcome the scarcity of single-phase multiferroics, recent work concentrates on the class of composite-type artificial multiferroics or thin film nano-/heterostructures [2-6]. Amongest, one of the composite-type structures is the nanostructure of ferro/ferri magnetic nanoparticles embedded/distributed in a ferroelectric matrix so called nanocomposite thin films [5]. As the nanocomposite thin films have large interaction area and remarkable tunability between ferroelectric and magnetic order parameters, thus are of great interest [5-8]. This approach opens a new door for developing mulltiferroics nanostructures by tailoring the volume fraction of magnetic content [7, 9]. Several investigations based on ferroelectric–ferrite nanocomposite thin films including $BiFeO_3$ (BFO), $BaTiO_3$ (BTO) and $PbTiO_3$ (PTO) as ferroelectric constituents and $CoFe_2O_4$(CFO) and $NiFe_2O_4$(NFO), as ferrimagnetic constitute have been reported in literature showing both ferroelectric and ferromagnetic properties [8-11].

Among the perovskite based oxides, BFO is a room temperature (*R*-*T*) multiferroic (T_C = 1123 K and T_N = 643 K), and has been widely studied in literature [6, 12, 13]. It exhibits good ferroelectric properties with large value of remnant polarization (P_r) in thin film form [12, 13]. However, weak magnetic behaviour of BFO limits its use for multifunctional device based applications [14]. This week magnetism in BFO can be improved by modification with ferrite oxides [7, 9, 10]. Among ferrites, CFO, NFO are the largely studied magnetic oxide material in literature [9] and have been widely used as the magnetic component for developing multiferroic nanocomposite thin films

2. Methodology

High purity bismuth nitrate [$Bi(NO_3)_3.5H_2O$], cobalt nitrate $Co(NO_3)_2.6H_2O$, nickel nitrate $Ni(NO_3)_2.6H_2O$, iron nitrate [$Fe(NO_3)_3.9H_2O$ and 2-methoxyethanol of Sigma Aldrich (99.99%) were used for synthesis. In the first step, BFO and NFO precursor solutions were individually prepared by standard sol-gel method. In the second step, both precursor solutions of BFO and NFO were mixed together with volume ratio of (1-*x*)BFO-*x*NFO/CFO (*x* = 0, 0.1, 0.2, 0.3) using Hamilton microliter microsyringe, heated and stirred continuously at 70 °C for 1 hours to get a well mixed BFO-CFO/NFO gel solution. The mixed solution was spin coated onto indium tin oxide coated (ITO) glass substrate at 3000 rpm for 40 seconds and subsequently baked at 300 °C for 5 minutes. Finally the thin films were obtained by repeating this spin-coating-baking-annealing process twice. The films were annealed at 600 °C for 30 min in ambient atmosphere.

3. Characterization techniques

Phase analysis of the samples were done by X-ray diffraction (XRD) using CuKα radiation (λ = 1.54178Å) (Philips X-pert PRO). The cross-section of the films were analyzed with scanning electron microscope (SEM) Zeiss EVO-50 ESEM (Carl *Zeiss* SMT, Inc., New York). The microstructure of the BFO/NFO nanocomposite thin films was observed by plane view transmission electron microscopy (TEM TECNAI G2 20 S-TWIN).The standard ion beam milling procedure was adopted to prepare TEM sample. Surface morphology of the films were studied by Atomic force microscopy (AFM) model (NT-MDT SOLVER NEXT). For electrical measurements, the Au dots of 0.8 mm were deposited using the mask on the film by sputtering technique. Room temperature (*R-T)* Dielectric and polarization-electric field *(P-E)* loops were measured using HP 4192A impedance analyzer and ferroelectric tester (Radiant Precision

Premier II Technology). Magnetization-applied magnetic field (*M-H*) loops were measured using a superconducting quantum interference device (SQUID) (Quantum Design's MPMS XL7).

4. Results and discussions of (Pure BFO) thin films

Single phase polycrystalline BFO thin films were prepared by sol-gel spin coating method followed by annealing at different temperature. Structural, optical and ferroelectric behavior of sol-gel driven $BiFeO_3$ thin films has been systematically investigated.

Figure 1 shows the X-ray diffraction (XRD) pattern of BFO thin films annealed at different temperature (500, 550, and 600ºC for 1 h). All the XRD peaks in the pattern corresponds to perovskite-type rhombohedral structure with space group R3c (N◦. 161) which agrees with the respective Inorganic Crystal Structure Data Base Nº. 86-1518[14]. The intensity of the peaks is increasing with annealing temperature, which suggests higher crystallization in the films annealed at high temperature. The average grain size as calculated by Scherrer formula, are ~ 52 nm and ~ 83 nm for films annealed at 500°C and 600°C respectively. No other impurity phases such as $Bi_{25}FeO_{40}$ and $Bi_{46}Fe_2O_{70}$ are observed.

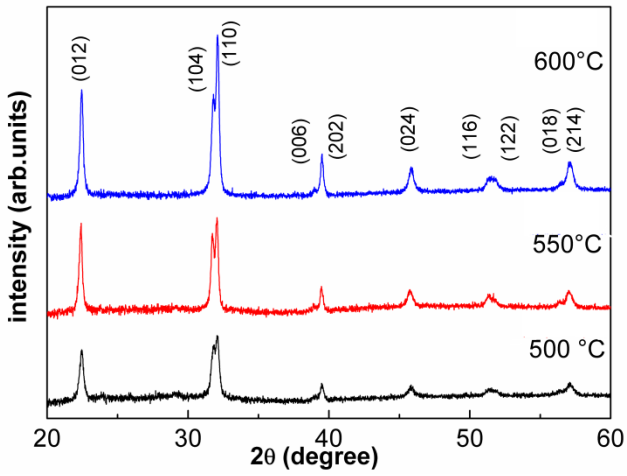

Fig. 1 XRD pattern of BFO thin films annealed at different temperature.

Figures 2 (a,b) illustrate the FE-SEM images of BFO thin films annealed at 500^{o}C and 600^{o}C respectively. BFO thin film annealed at 500^{o}C indicates equiaxed grains with uniform size distribution; however, few pores are also observed in the films (white circle in Fig. 2a). The film annealed at 600^{o}C shows inhomogeneous grain growth caused by the formation of irregular grains. The results are consistent with the previously reported results for BFO thin films [15, 16]. The average grain size of the films annealed at 500°C to 600°C are ~ 62 nm and ~ 90 nm respectively. The smaller grain size values, as calculated from XRD, is due to the peak broadening from structural defects and stress in the thin films [15]. Fig. 2 (c) shows the cross-sectional image of BFO thin film, the thickness of the film is determined to be ~200nm.

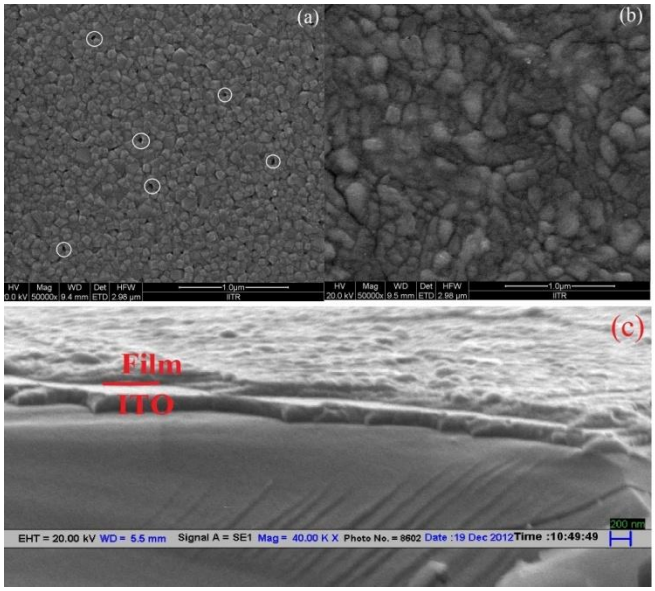

Fig. 2 FE-SEM images of BFO thin films annealed at (a) 500^{o}C, (b) 600^{o}C and (c) shows the cross section image of film.

Figures 3(a-c) illustrate the two dimensional AFM image of BFO thin films annealed at 500^{o}C, 550^{o}C and 600^{o}C respectively. It is evident that increasing annealing temperature, smaller grain

coalesce to for form bigger elongated grains. The root mean square roughness (*Rq*) values are measured using the 10 μm x 10 μm area for better statics and found to increase with temperature. The *Rq* values are ~ 5.32nm and ~9.63nm for the films annealed at 500^{o}C and 600^{o}C respectively. The increase in *Rq* values with innealing temperature is mainly atributed to the increse in grain size [15].

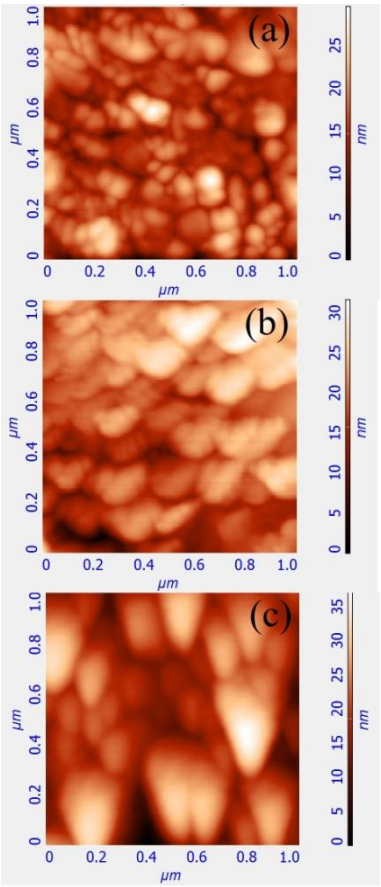

Fig. 3 AFM images of BFO thin films annealed at (a) 500^{o}C, (b) 550^{o}C and (c) 600^{o}C.

Figure. 4(a) shows transmittance spectra of BFO thin films annealed at different temperature, in the wavelength range from 400 to 900 nm. The wavy nature of the transmittance away from the fundamental absorption edge is due to the interference arising from the substrate - film interface. Obviously, the transmittance for all the films decreases to zero in the wavelength range of 200-

450 nm. It is clearly seen that the BFO films are highly transparent with transmittances in the visible and near-infrared wavelength region. The transmittance spectra of the films annealed at 500°C show interferences fringes and high transparency (85%) that decreases with increasing annealing temperature. A significant decrease in transmittance spectra in UV-*vis* region is attributed to the increase in roughness with annealing temperature that lead to the absorption and scattering of light [15, 17].

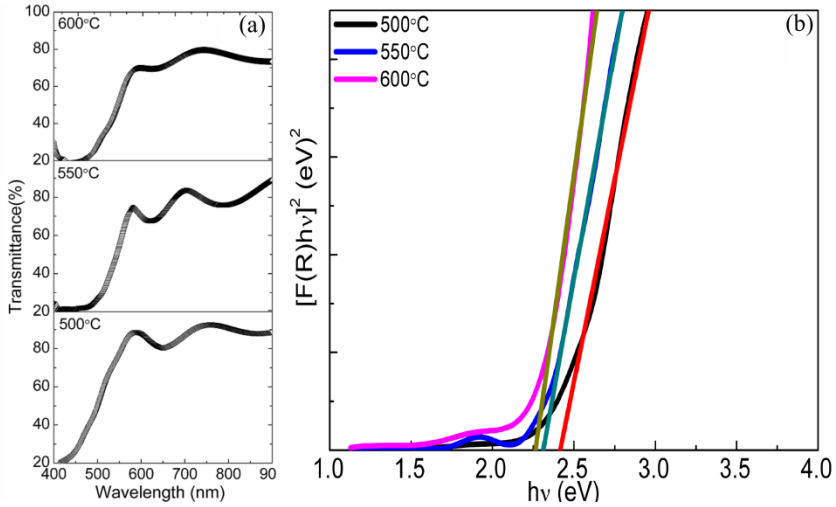

Fig. 4 (a) UV-visible transmission spectra (b) $[\alpha h\nu]^2$ vs $h\nu$ plots for determination of E_g of BFO thin films annealed at different temperature.

The E_g of BFO thin films was determined by the equation.

$$(\alpha h\nu)^2 = A(h\nu - E_g) \quad (1)$$

where, $h\nu$ is the incident photon energy, α is absorption coefficient, A is constant relative to the material. For the E_g calculation the straight portion $(\alpha h\nu)^2$ vs photon energy $(h\nu)$ plots have been extrapolated (Fig. 4(b)). The E_g of the films annealed at 500°C, 550°C, and 600°C are determined to be 2.42, 2.31 and 2.27 eV respectively. The difference in E_g with annealing temperature was

believed to be originated from the larger grain boundary fraction in smaller grains. The larger potential barriers at the grain boundaries caused the absorption edge toward the shorter wavelengths (higher energy) [15]. The reported value of band gap by chen *et. al* is 2.71 eV for the sol-gel derived BFO thin films [18], the lower E_g values suggest the improved crystallization and homogeneity of the films [19]. The difference of E_g with annealing temperature found to be consistent to be reported by Tyagi [20] and Boby Singh [15]. The value of the E_g of the BFO thin films annealed at 500°C is nearly equal to those reported by F. Gao et al. (2.5 eV) and L. Bi et al. (2.44 eV) [26, 27] and lower than those reported by other workers [18, 19]. Table 1 summarizes the comparison between observed and reported properties for BFO samples.

Fig.5 (a) and (b) shows the *RT* frequency dependent dielectric constant (ε′) and dielectric loss (ε″) of BFO films in the frequency range of 100 Hz to 10 kHz. The ε′ increases with increasing annealing temperature and found 181, 198 and 209 (at100Hz) for films annealed at 500^{o}C, 550^{o}C, 600^{o}C kHz, respectively. The grain growth, improved crystallinity and higher density of the films may be the reason for increased ε′. With increasing frequency, ε′ gradually decreases for all films. The results are comparable with BFO thin films prepared by different technique (Table 1) [23-25]. As shown in Fig. 5(b), a lower ε″ are observed in the films annealed at higher temperature. Slight increases in ε″ are also observed in the high frequency region (10^5-10^6 Hz). Such frequency dependent ε′ and ε″ behaviour of BFO thin films is expected, by considering the space charges, interface and dielectric relaxation in ferroelectric thin films.

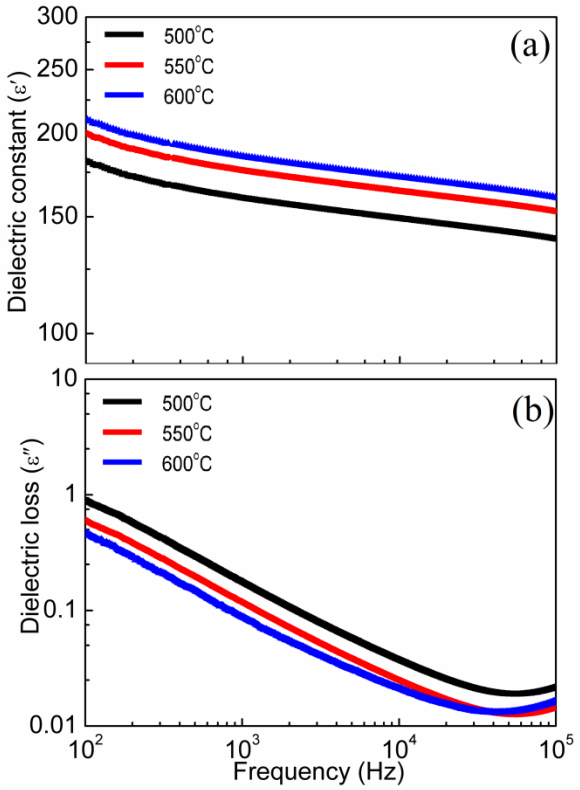

Fig. 5 The frequency dependent (a) ε′ and (b) ε″ of BFO thin films annealed at different temperature.

Fig. 6 shows the temperature dependence ε′ behaviour of BFO thin films annealed at 500 °C. The measurement are carried out in frequency and temperature range of 1 kHz ≤ f ≤ 500 kHz, and 20°C ≤ T≤ 300 °C respectively. It can be seen that ε′ increases with the increasing temperature and then decreases above ~ 270°C. As the temperature increases, more charge carriers get excitation from their trapping centres and contribute to the polarization which in turn increases the ε′ of the films. The higher rate of increase in ε′ at 100 Hz is due to the contribution from surface polarization which diminishes at higher frequencies. The anomaly in ε′ around T_N signifies the antiferromagnetic phase of BFO is coupled to the electric polarization which is essential for a multiferroic system [6, 26]. Similar behaviour are also observed for the film annealed at 550°C and 600°C temperature.

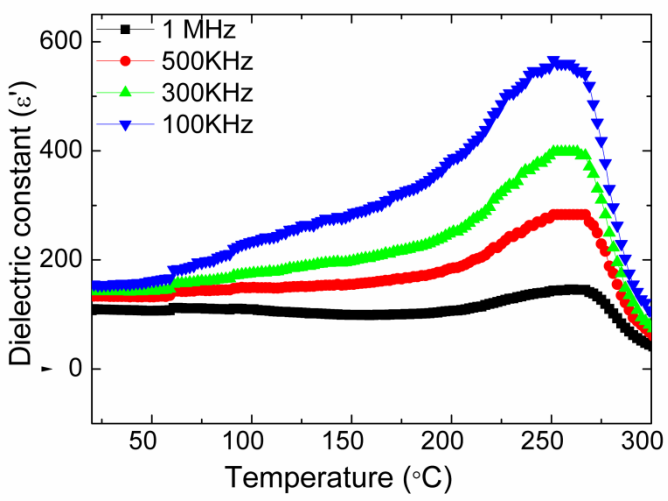

Fig. 6 Temperature dependent ε′ of BFO thin films annealed at 500°C with different frequencies.

Fig. 7 shows the *R-T* polarization vs applied electric field (*P-E*) hysteresis loops of BFO thin films annealed at different temperature. The films annealed at 500°C shows well saturated *P-E* loop, however, increasing annealing temperature from 500°C to 600°C, the $2P_r$ value decreased from ~51 μC/cm^2 to ~40 μC/cm^2 respectively. There are several factors contribute to the variation in ferroelectric properties including the Bi volatility, the nucleation and grain growth etc. of the BFO phase. The higher annealing temperature promotes nucleation and grain growth of the films which reportedly improves the ferroelectric properties [24, 26, 27]. However in the present case, the decreasing trend of ferroelectric properties may be dominated by volatility of Bi at higher annealing temperature which may lead to the formation of vacancy defects and degrades the ferroelectric properties of BFO thin films.

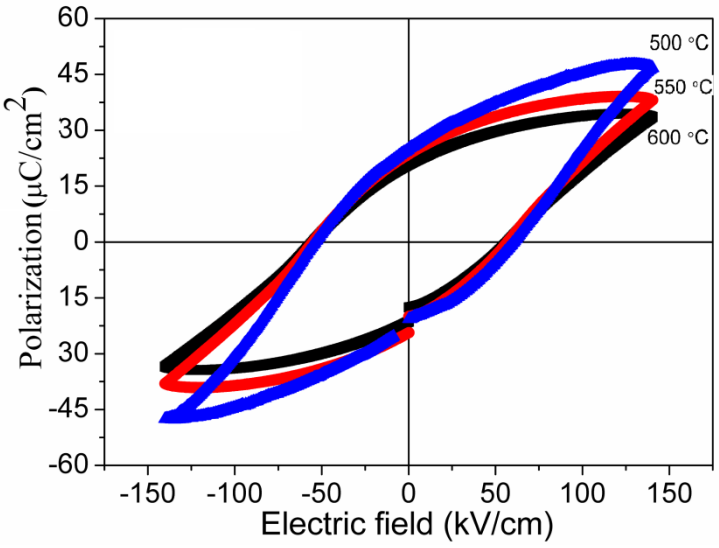

Fig. 7 *P-E* loops of BFO thin films annealed at (a) 500^{o}C, (b) 550^{o}C and (c) 600^{o}C.

References:

[1]. N.A. Spaldin, M. Fiebig, Science **309**, 391-392 (2005)

[2]. W. Eerenstein, N. D. Mathur, and J. F. Scott, Nature (London) **442,** 759-765 (2006)

[3]. T. Kimura, T. Goto, H. Shintani, K. Ishizaka, T. Arima, Y. Tokura, Nature (London) **426,** 55-58 (2003)

[4]. D. Lebeugle, D. Colson, A. Forget, M. Viret, A.M. Bataille, A. Gukasov, Phys. Rev. Lett. **100,** 227602 (2008)

[5]. Y. Li, Y. Fan, H. Zhang, X. Teng, X. Dong, H. Liu, X. Ge, Q. Li, W. Chen, X, L.Z. Ge J. Supercond. Nov. Magn. **27** 1239–1243 (2014

[6]. M. Muneeswaran, P. Jegatheesan, M. Gopiraman, Ick-Soo Kim, N.V. Giridharan Appl. Phys. A **114** 853–859 (2014)

[7]. J. Wang, J. B. Neaton, H. Zheng, V. Nagarajan, S. B. Ogale, B. Liu, D. Viehland, V. Vaithyanathan, D.G. Schlom, U.V. Waghmare, N.A. Spaldin, K.M. Rabe, M. Wuttig, R. Ramesh, Science **299,** 1719-1722 (2003)

[8]. J. Wang, H. Zheng, Z. Ma, S. Prasertchoung, M. Wuttig, R. Droopad, J. Yu, K. Eisenbeiser, R. Ramesh, Appl. Phys. Lett. **85,** 2574-2576 (2004)

[9]. Q. Man, W. Sun, F. Yang, C. Qiu, Y. Zhao, G. Hu J Mater Sci: Mater Electron **25** 1269–1274 (2014)

[10]. Z. Simoes, L.S. Cavalcante, F. Mourac, E. Longo, J.A. Varela J. Alloy. Compd. 509 5326–5335 (2011)

[11]. X. S. Xu, T. V. Brinzari, S. Lee, Y. H. Chu, L. W. Martin, A. Kumar, S. McGill, R. C. Rai,,R. Ramesh, V. Gopalan, S. W. Cheong, and J. L. Musfeldt Phys. Rev. B **79**, 134425 (2009)

[12]. Z. Lin, W. Cai, W. Jiang, C. Fu, C. Li, Y. Song, Ceram. Int. 39, 8729–8736 (2013)
[13]. C. A. Raj, M. Muneeswaran, P. Jegatheesan, N. V. Giridharan , V. Sivakumar, G. Senguttuvan J Mater Sci: Mater Electron **24** 4148–4154 (2013)
[14]. Simões A.Z, Cavalcante L.S, Moura F, Batista N.C, Longo E, Varela J.A. Appl. Phys. A. **109** 703–714 (2012)
[15]. B. S. Soram, B.S. Ngangom, H.B. Sharma, Thin Solid Films **524** 57-61(2012)
[16]. L. S. Cavalcante, J. C. Sczancoski, F. S. De Vicente, M. T. Frabbro, M. Siu Li, J. A. Varela E. Longo J Sol-Gel Sci Technol **49** 35–46 (2009)
[17]. M. Diana, M. Tasca, M. Delibas, G.I Rusu Applied Surface Science **156** 200–206 (2000)
[18]. X. Chen, H. Zhang, T. Wang, F. Wang, W. Shi, Phys status solidi A **209** 1456-1460 (2012)
[19]. Y. Xu, M. Shen, Materials Letters **62** 3600-3602 (2008)
[20]. P. Tyagi, A. G. Vedeshwar, Bull. Mater. Sci. **24** 297-300 (2001)
[21]. F. Gao, Y. Yuan, K.F. Wang, X.Y. Chen, F. Chen, J.M. Liu, Z.F. Ren Appl. Phys. Lett. **89** 102506 (2006)
[22]. L. Bi, A.R. Taussig, H.S. Kim, L. Wang, G.F. Dionne, D. Bono, K. Persson, G. Ceder, Ross C.A Phys. Rev. B **78** 104106 (2008)
[23]. R.Y. Zheng, J. Wang, S. Ramakrishna J. Appl. Phys. **104** 034106 (2008)
[24]. A. Z. Simoes, L. S. Cavalcante, C. S. Riccardi, V. J. A, E. Longo (2007) J. Sol-Gel Sci. Technol. 44:269–273
[25]. A.Z. Simões · L.S. Cavalcante · F. Moura · N.C. Batista · E. Longo · J.A. Varela Appl Phys A (2012) 109:703–714
[26]. R. Mazumder, P. Sujatha Devi, Dipten Bhattacharya, P. Choudhury, A. Sen, M. Raja, Appl. Phys. Lett. **91** 062510 (2007)
[27]. S.K. Singh, Y.K. Kim, H. Funakubo, H. Ishiwara, Appl. Phys. Lett. **88** 162904 (2005)

4.1 Results and discussions of (BFO-CFO) nanocomposite thin films

We have studied to investigate the feasibility of effectively combining BFO and CFO/NFO phases, using sol-gel process in which the precursor of both the ferroelectric and ferrimagnetic phases were mixed before spin coating. The spin coating of the mixed precursor solutions of the BFO and CFO/NFO phases allow for nanoscale mixing of subsequent composite phases. We have observed strong effect of the volume ratio of cobalt ferrite on the magnetic behavior of such BFO/CFO nanocomposite thin films.

Figure 1 shows the XRD patterns of pure BFO and BFO/CFO nanocomposite thin films. XRD pattern of BFO is well indexed with rhombohedral symmetry, while the XRD of BFO/CFO shows the well defined peaks of pervoskite BFO phase with sharp (110) peak and other to the cubic spinel CFO phase. It is evident from the patterns that as the volume fraction of CFO increases, the intensity of the peaks corresponding to cubic spinel phase become stronger. Additionally, the pattern indicates that both phases BFO and CFO are polycrystalline in nature and have no preferential crystallographic orientations. The average crystallite size of both BFO and CFO was calculated from XRD peak broadening using Scherer's formula and found to be 28.80 nm and 14.12 nm respectively.

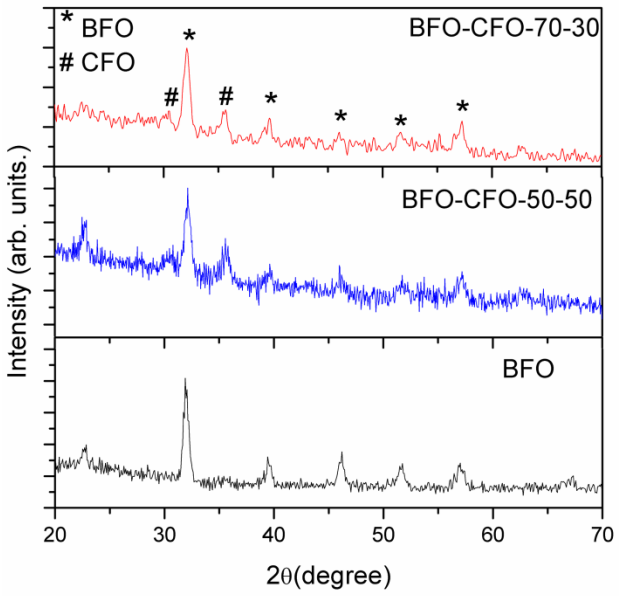

Fig. 1. X-ray diffraction pattern of multiferroic pure BFO and BFO/CFO nanocomposite thin films.

Figure 2(a) and 2(b) shows the AFM images of pure BFO and BFO/CFO films. It clearly shows that the BFO/CFO (70/30) films consist of randomly distributed fine CFO particles in BFO matrix. Figure 3(a) shows cross sectional SEM image of BFO/CFO (0.5/0.5) film deposited on

ITO coated glass substrate. The cross section SEM image reveal clear boundary between BFO/CFO film and ITO coating. The thickness of the composite film and ITO coating was 170 nm and 150 nm respectively. Figure 3(b) shows the EDX_S of BFO/CFO (0.5/0.5) nanocomposite thin films. The presence of Bi, Co, and Fe elements at nearly expected elemental composition was confirmed.

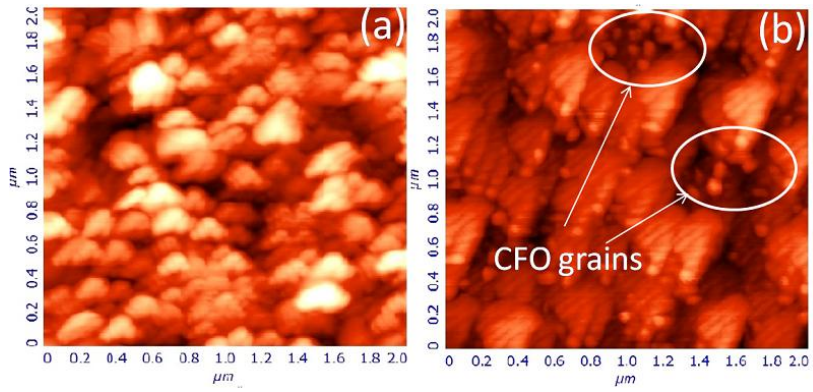

Fig. 2. (a) and (b) AFM micrographs of the pure BFO and BFO/CFO nanocomposite thin films.

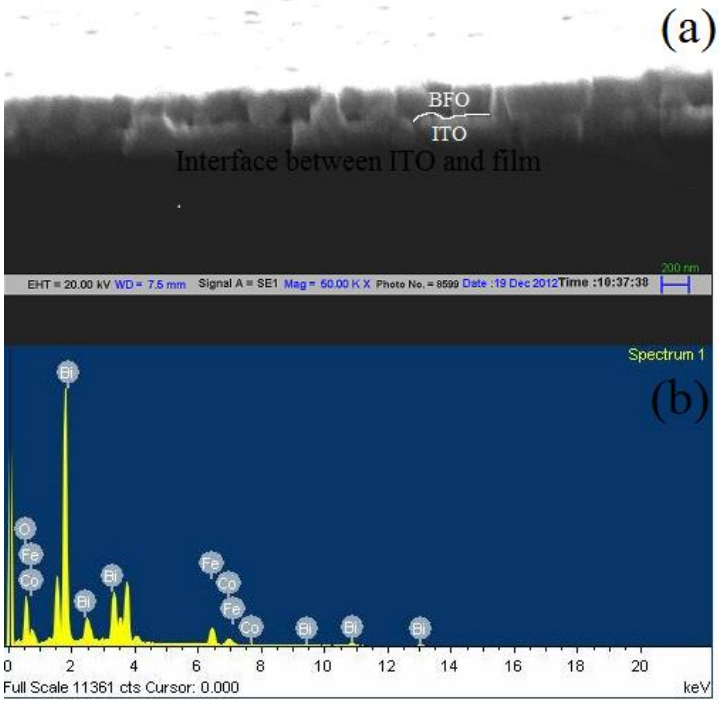

Fig. 3. (a) and (b) shows the cross section SEM micrographs and energy dispersive X-ray spectra of the BFO-CFO nanocomposite thin films respectively.

Figure 4 shows the TEM image of the BFO-CFO-70-30 composite thin film. Figure... clearly depicts two phases, the dark particles indicated by white circles in figure were the CFO grains and the light particles indicated by the yellow circles were the BFO grains. Therefore, it was concluded that the CFO grains were randomly distributed in BFO matrix.

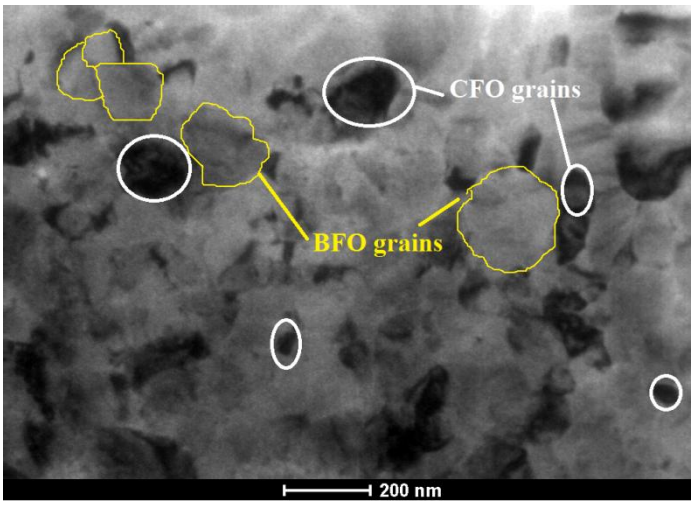

Fig.4. Enlarge TEM image of the BFO-CFO thin film.

Figure 5 (a) shows the in plane *M-H* behavior of all the samples with varying volume concentration of CFO at 300K. Pure BFO thin film clearly shows the antiferromagnetic behavior. Whereas, the well defined magnetic hysteresis loop was observed in BFO/CFO nanocomposite thin films. The concentration of CFO strongly affects the magnetic properties of BFO/CFO. The M_s, M_r and coercivity (H_c) values of BFO/CFO nanocomposite thin films are found to increase with increase in the CFO concentration.The maximum value of M_s and M_r is ~ 196 emu/cc and 22.8 emu/cc respectively for x=0.50 concentration. It is also evident that coercivity increases

sharply for x=0.5 (inset fig 4). This could be attributed due to magnetoelastic coupling between antiferromagnetic BFO and ferromagnetic CFO phase [1], [2], [3**].**

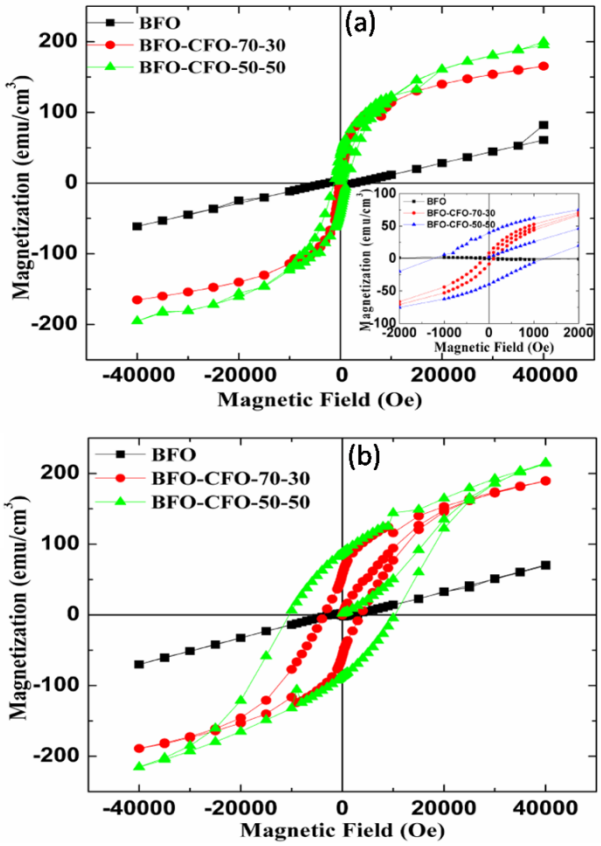

Fig.5. Magnetic hysteresis loops of pure BFO and BFO/CFO nanocomposite thin films at (a) 300K and (b) 100k.

Figure 5(b) shows the *M-H* hysteresis loops measured at 100 K. The M-H loop of BFO-CFO-70-30 exhibit a discontinuous change (shoulder) due to the dominant antiferromagnetic nature of the curve. However, BFO-CFO-50-50 shows a single phase hysteresis loop indicating a typical ferromagnetic nature of the films [4]. The values of M_r, and M_s increase significantly with decreasing temperature due to the suppression of thermal fluctuation of magnetic dipoles at low

temperature. A large H_c of 10.5 KOe was observed at 100K which suggests that presence of an exchange interaction between BFO and CFO grains is dominant at low temperature.

Figure 6 shows the polarization vs. applied electric field (*P*-*E*) hysteresis loops of the pure BFO and the BFO/CFO nanocomposite thin films measured at room temperature as a function of CFO concentration at 1Hz. The BFO and BFO/CFO (70/30) nanocomposite thin films show the desirable ferroelectric behavior. The remanent polarization (P_r) value measured for the pure BFO and 0.7BFO-0.3CFO thin film are 15μC/cm^2 and 10μC/cm^2 respectivity, which are comparable to the previously reported values for thin films prepared by sol-gel method [5]. Larger electric coercive field was observed in nanocomposite BFO/CFO (50/50) than the pure BFO. The paraelectric cobalt ferrite phase is responsible for the decrease in the ferroelectric properties.

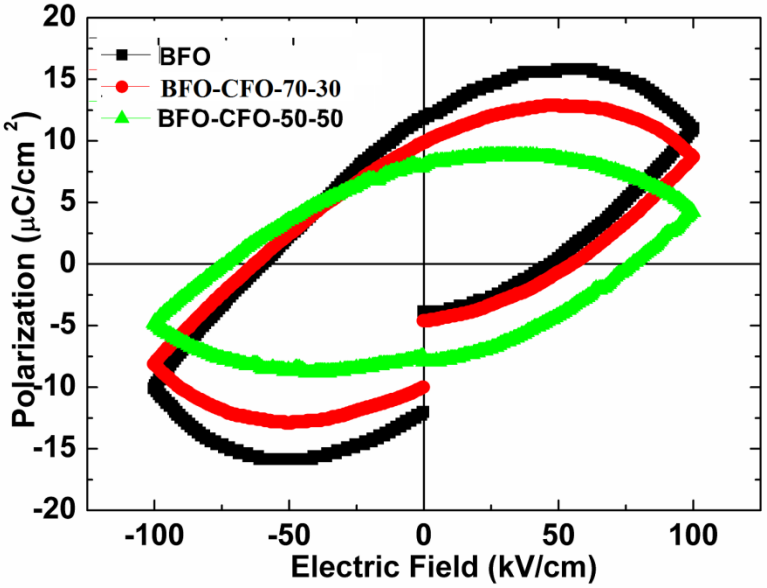

Fig. 6. Polarization-electric field hysteresis loops of pure and BFO./CFO nanocomposite thin films.

Figure 7 shows the room temperature leakage current characteristic of the pure BFO and BFO-CFO composite thin films as a function of increasing CFO volume ratio. Under positive and negative applied fields of 100 kV/cm, the leakage current densities were measured. The leakage current increases with increasing CFO volume ratio, which is accounted by the low electrical resistance of CFO grains. It is also clear from the figure.... that the deterioration in ferroelectric behaviour is due to high leakage current density.

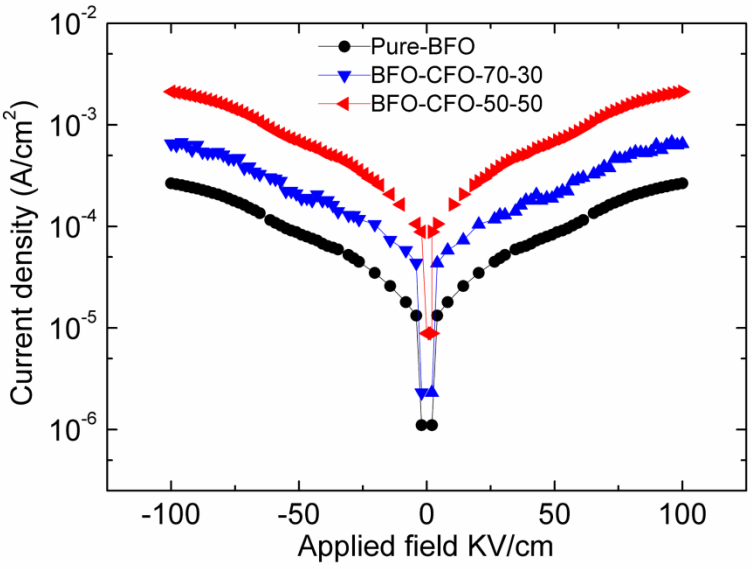

Fig. 7. Leakage current behaviour of BFO and BFO-CFO composite thin films.

Figure 8 shows the frequency dependence dielectric constant of both pure BFO and BFO/CFO nanocomposite films at room temperature. There are many factors which can affect the dielectric behavior of the ferrite materials such as grain size, cation distribution, porosity, crystal defects and method of sintering etc [6], [7]. In a low frequency regime, interfacial/surface polarization plays a dominant role in determining the dielectric properties of nanoferrite materials [8]. The

contribution from surface polarization, at low frequency which gives an initial high value that decays rapidly with frequency as it cannot follow the higher applied frequency.

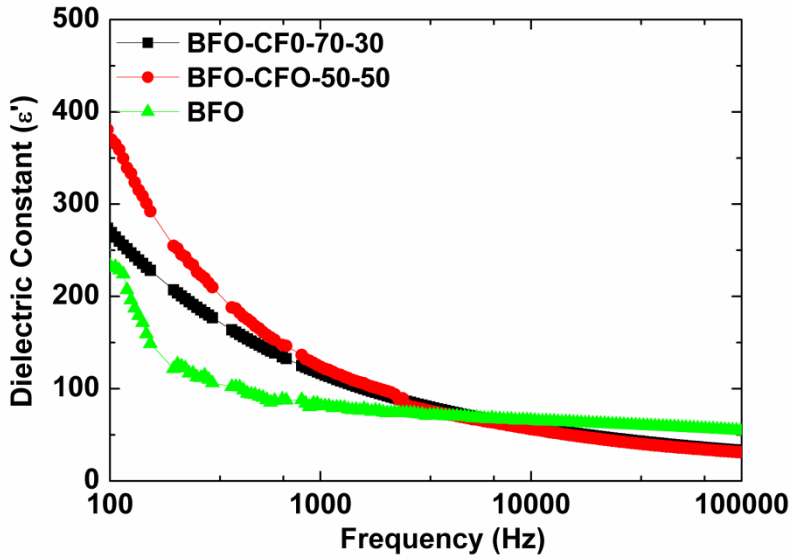

Dielectric constant of BFO and BFO/CFO nanocomposite thin films.

References:

[1]. Sone, Sho Sekiguchi, Hiroshi Naganuma, Takamichi Miyazaki, Takashi Nakajima, "Magnetic properties of $CoFe_2O_4$ nanoparticles distributed in a multiferroic BiFeO3 matrix," *J. Appl. Phys.*, vol. 111, pp. 124101-1-124101-5, 2012.

[2]. H. Zheng, J. Wang, S.E. Lofland, Z. Ma, L.M. Ardabili, T. Zhao,L.S. Riba, S.R. Shinde, S.B.Ogale, F. Bai, D. Viehland, Y. Jia, D.G.Schlom, M.Wuttig, A. Roytburd, R. Ramesh, " Multiferroic $BaTiO_3$ $CoFe_2O_4$ Nanostructures," *Science.*, vol. 303, pp. 661-663, 2004.

[3]. Nicolas M. Aimon, Dong Hun Kim, Hong Kyoon, hoi, C. A. Ross, " Deposition of epitaxial $BiFeO_3$/CoFe2O_4 nanocomposites on (001) $SrTiO_3$" *Appl. Phys. Lett.*, vol. 100, pp. 092901, 2012.

[4]. V. Stancu, C. Dragoi, V. Kuncser, G. Schinteie, L. Trupina, E. Vasile, L. Pintilie., " The study of the electric and magnetic properties of $PbZr_{0.2}Ti_{0.8}$O3–BiFeO3 multilayers" *Thin solid films.*, vol. 519, pp. 6269-6277, 2011

[5]. Zuli Liu, Hongri Liu, Guihuan Du, Jian Zhang, Kailun Yao, "Electric properties of BiFeO3 films deposited on $LaNiO_3$ by sol-gel process," *J. Appl. Phys.*, vol. 100, pp. 044110-1-044110-4, 2006.

[6]. M. C. Dimri, A. Verma, S. C. Kashyap, D. C. Dube, O. P. Thakur, and C. Prakash, "Structural, dielectric and magnetic properties of NiCuZn ferritegrown by citrate precursor method," *Mater. Sci. Eng. B.*, vol. 133, pp. 42-48, 2006.

[7]. S. E. Shirsath, B. G. Toksha, and K. M. Jadhav, "Structural and magnetic properties of In^{3+} substituted $NiFe_2O_4$," *Mater. Chem. Phys.*, vol. 117, pp. 163-168, 2009.
[8]. Murthy V R K, Sobnandari, " Dielectric properties of some nickel-zink ferrites at radiao frequency," *J Phys. Status Solidi a.*, vol. 36, pp.133-137, 1976.

4.3 Results and discussions of (BFO-NFO) nanocomposite thin films

In this part of the report we have studied to investigate the feasibility of effectively combining BFO and NFO phases, using sol-gel process in which the precursor of both the ferroelectric and ferrimagnetic phases were mixed before spin coating. The spin coating of the mixed precursor solutions of the BFO and NFO phases allow for nanoscale mixing of subsequent composite phases. We have observed strong effect of the volume ratio of nickel ferrite on the magnetic behavior of such BFO/NFO nanocomposite thin films.

Fig. 1 displays the XRD pattern of bare indium tin oxide (ITO) substrate, BFO, NFO and BFO/NFO nanocomposite thin films after annealing at 600ºC. The XRD patterns of BFO and NFO exhibit the prominent peaks are indexed of perovskite BFO and the cubic spinel symmetry NFO respectively. At the same time, the peaks corresponding to NFO in BFO/NFO composite thin films spectra were hard to see due to superimposition of NFO peaks with both BFO and ITO peaks. Moreover, due to the low volume ratio of NFO as compared to BFO, the NFO grains were trapped around around the ferroelectric grains of BFO phase, and its growth was found to be restrained [1]. As a result of which no prominent diffraction peak for spinel NFO was seen in the XRD spectrum of BFO/NFO composite thin films.

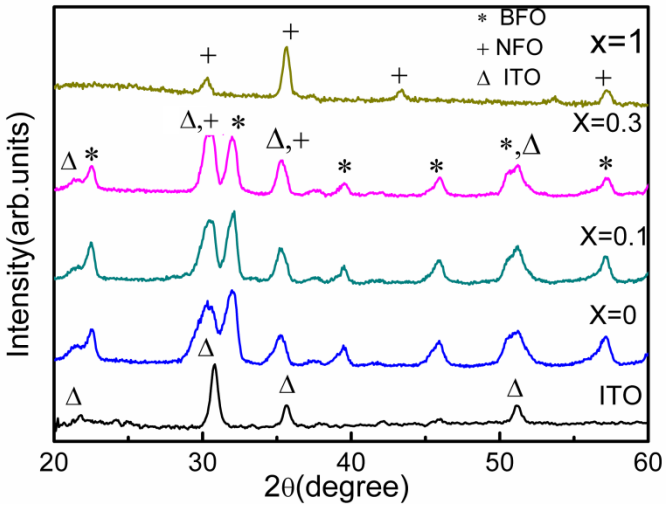

Fig. 1 XRD pattern of BFO, NFO and BFO/NFO nanocomposite thin films.

To further confirm the crystallisation of NFO phase in composite thin film, TEM analysis was done. Fig. 2(a) shows the plane view TEM image of BFO/NFO (x=0.1) nanocomposite thin film and Fig. 2(b) shows the corresponding selected area diffraction pattern. Fig. 2(a) clearly depicts that NFO having lighter Ni atoms appear dark, is embedded in BFO matrix which appears bright because of containing heavier Bi atoms, indicating nanoscale mixing of the BFO and NFO phases [2]. The diffraction spots of both BFO and NFO were also observed in selected are diffraction pattern of BFO/NFO nanocomposite thin film structure indicating the distribution of BFO and NFO particles in the area. The calculated d_{hkl} values as per the respective diffraction ring shown in Fig. 2(b) for BFO and NFO are found to be d_{110} = 0.279 nm, and d_{311} = 0.250 nm respectively. Fig. 2 (c) shows the cross-sectional image of BFO thin film, the thickness of the film is determined to be ~200nm.

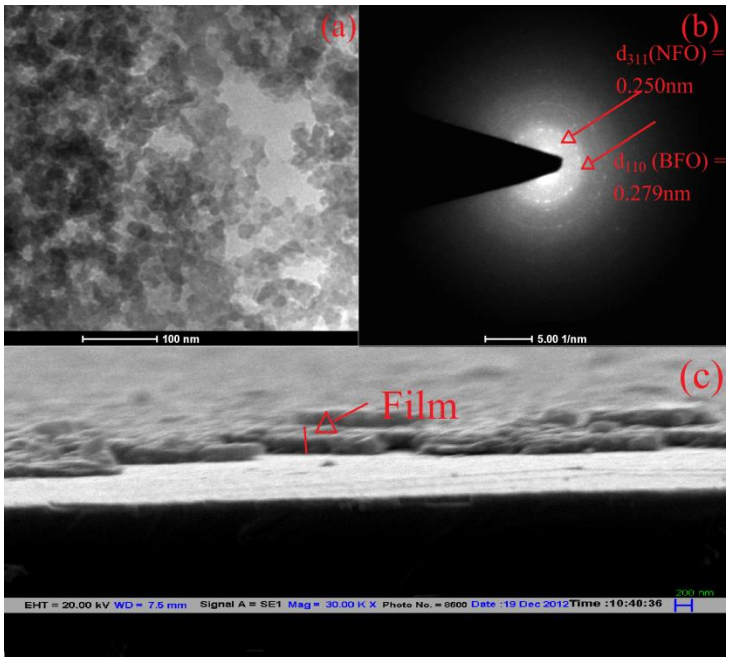

Fig. 2 (a) In plane TEM image of BFO/NFO nanocomposite thin films (b) selected area diffraction pattern of BFO/NFO composite thin films and (c) shows the cross section image of film.

Fig. 3 (a), (b) and (c) showed the surface morphology of BFO, NFO and BFO/NFO (x=0.1) thin films obtained from the atomic force microscopy (AFM). The micrograph suggests the films were dense and well crystallized. The introduction of NFO grains in BFO matrix greatly affect the surface morphology of BFO thin films. Particularly, the fine grain size and lower roughness value of the BFO/NFO nanocomposite thin films were observed as compared to BFO thin films. The root mean square roughness (*Rq*) values were measured using the 10 μm x 10 μm area for better statics and found to decrease for composite thin films as compared to BFO. The *Rq* values were ~9.32nm, ~6.29 and ~5.33 nm for BFO, BFO/NFO and NFO thin films respectively.

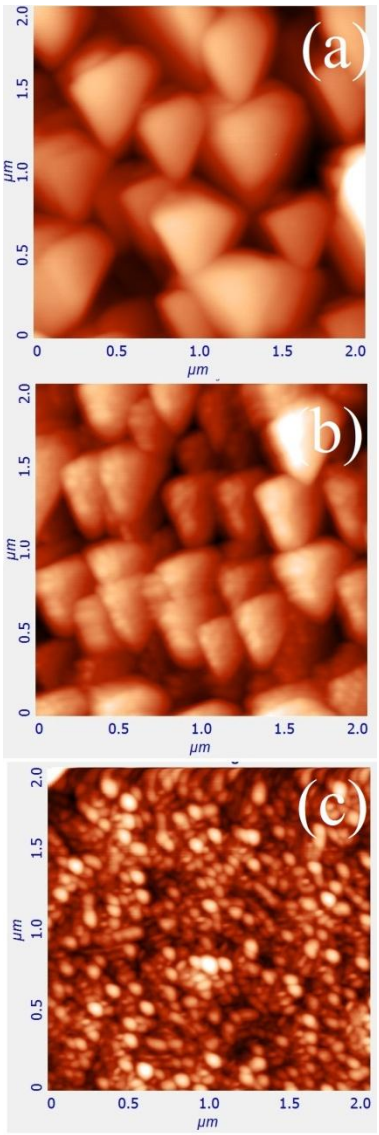

Fig. 3 AFM images of (a) BFO (b) BFO/NFO and (c) NFO thin films.

Fig. 4 (a) shows the in plane *M-H* behaviour of BFO and BFO/NFO (x=0.1) nanocomposite thin films at 300K. BFO sample typically exhibit the anti-ferromagnetic behaviour due to its magnetism arises from self-canted spin magnetic moments of Fe^{3+}. Whereas, the well saturated *M-H* loop was observed for BFO/NFO nanocomposite thin films. This indicates that the major contribution to magnetic moment of the BFO/NFO nanocomposite thin films mainly arises from NFO. The saturation magnetization (M_s) and remnant magnetization (M_r) were found to be as high as ~ 34 emu/cm^3 and ~ 7 emu/cm^3 respectively for x = 0.1. This suggests that the

ferromagnetic character of the composite sample is sustained with NFO content ~ 0.1 in our samples. The magnetic data of the BFO/NFO nanocomposite thin films demonstrates that the magnetic properties can be quite tuned in the composites.

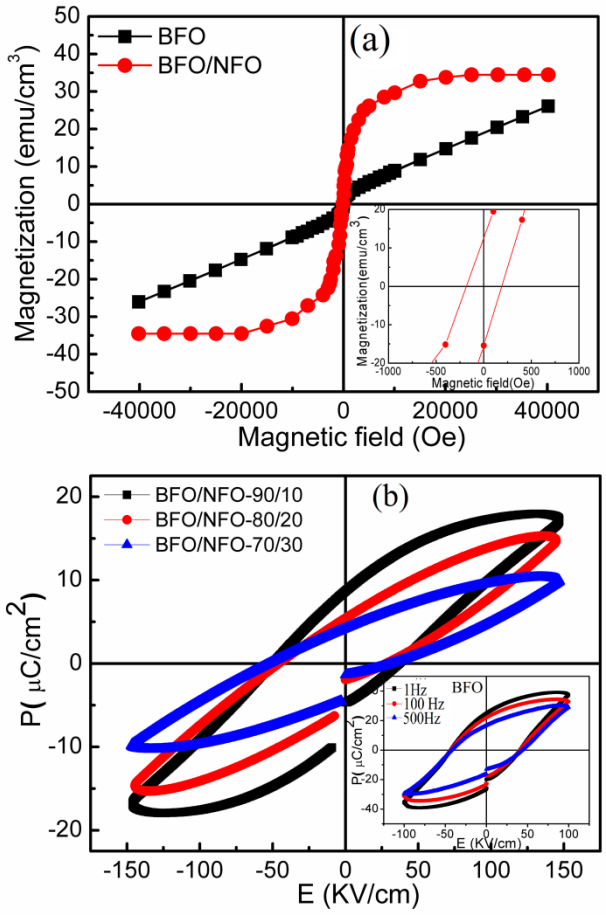

Fig. 4 (a) Magnetic hysteresis loops of BFO and BFO/CFO(x = 0.1) nanocomposite thin films at 300K and the inset is zoom view of the central part of the figure and (b) *P-E* loops of BFO and BFO/NFO nanocomposite thin films. Inset of Fig. 4(b) shows the P-E loops of x=0 sample at different frequencies.

Fig. 4(b) displays the *R-T* polarization-electric field (*P-E*) loops for (1-x)BFO–xNFO (x=0, 0.1, 0.2, 0.3) nanocomposite thin films measured at maximum field of 150 kV/cm. All samples shows non-saturated hysteresis loops due the leakage current [3]. The polarization continuously decreases with increasing NFO content. Inset of Fig. 4(b) shows the *P-E* loops for BFO

measured at 1Hz, 100 Hz and 500 Hz respectively. It can be observed that polarization values decreases with frequency, demonstrating the frequency dependent ferroelectric behaviour of the samples. Similar frequency dependent ferroelectric behaviour are observed for remaning samples in our series (not shown) and in accordance with previously reported frequency dependendent ferroelectric behaviour in BT-NFO based composite samples [4]. The value of P_r observed in our study is much higher than those reported by J. Gu et al. (P_r ~ 4.6 μC/cm^2) [5]. Particularly, the dominant lossy behaviour of *P-E* loop with x = 0.3 composite sample can be attributed to higher content of NFO, which lead to increase in conductivity of composite sample [6].

Fig. 5 (a) and (b) shows the *RT* frequency dependent dielectric constant (ε') and dielectric loss (tanδ) of (1-x)BFO–xNFO (x=0, 0.1, 0.2, 0.3) nanocomposite thin films measured at 1kHz. It can be observed that ε' for all the samples decreased with increasing frequency, from 100 Hz to 10 kHz. Particularly, in low frequency region, all the samples show frequency dispersion dielectric behaviour i.e. a rapid decrease in ε' with frequency and becomes almost constant, can be attributed due to well known interfacial polarization predicted by the Maxwell-Wagner model in conformity with koops phenomenological theory [7, 8]**.** However, ε' value for BFO thin films decreases slowly with increasing frequency as compared to BFO/NFO nanocomposite thin films, demonstrating the more frequency dependent dielectric behaviour of BFO in high frequency region and has higher ε' than BFO/NFO. In a low frequency regime, interfacial/surface polarization plays a dominant role in determining the dielectric properties of nanoferrite materials, which gives an initial high value that decays rapidly with frequency as it cannot follow the higher applied frequency. More importantly, in this study dielectric behaviour of BFO/NFO nanocomposite thin films is found to be higher than that of pure BFO film mainly in low frequency region; as the incorporation of NFO reduces the grain size of the films as confirm by

the AFM micrographs lead to an increase interfacial area and grain boundary resistance of composite material causing an additional interfacial polarization. As shown in Fig. 5(b), a gradual drop in tanδ are also observed in (1-*x*)BFO–*x*NFO(*x*=0, 0.1, 0.2, 0.3) thin films as the frequency increases. This kind of ε' and tanδ behaviour are expected for ferroelectric thin films and are in well agreement with those previously reported in literature for BFO/NFO based composites [9, 10].

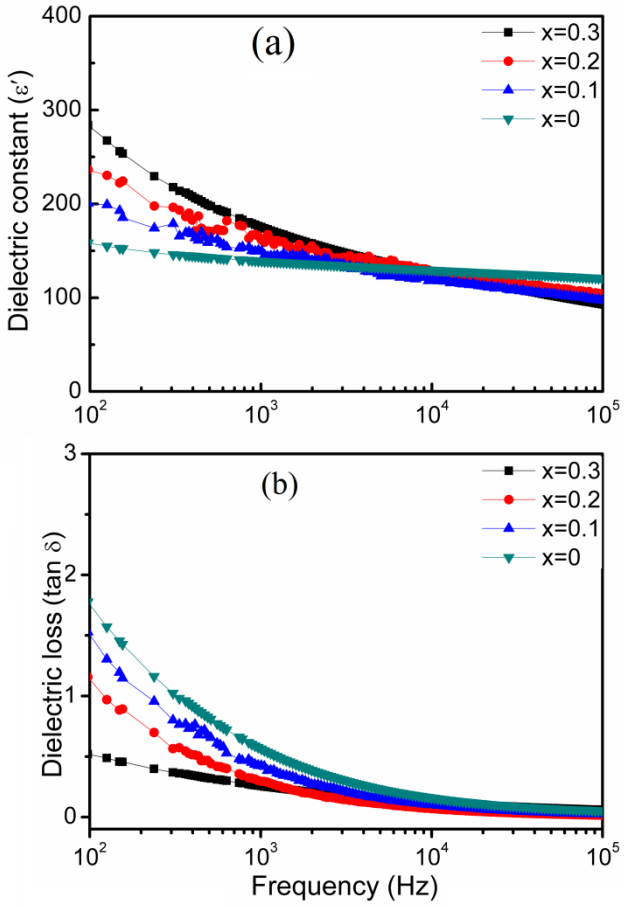

Fig. 5 (a) The frequency dependent dielectric constant of BFO and BFO/NFO nanocomposite thin films and (b) tan δ of BFO and BFO/NFO nanocomposite thin films.

1 Benatmane N, Crane SP, Zavaliche F, Ramesh R, and Clinton TW (2010) Appl Phys Lett 96:082503

2 Gu J, Yang S, Yang W, Qi Y, Zhao G, Sun H (2014) J Magn Magn Matter 349: 140–143

3 Tyagi M, Kumari M, Chatterjee R, Sun AC, Sharma P (2014)IEEE Trans Magn 50: 2500704

4 Zhan Q, Yu R, Crane SP, Zheng H, Kisielowski C, and Ramesh R (2006) Appl Phys Lett 89:172902

5 Scott JF (2008) J Phy : Condens Matter 20 021001

6 Upadhyay SK, Reddy VR (2013) J Appl Phys 113 114107

7 Koops CG (1951) Phys Rev 83:121

8 Wagner KW (1993) Ann Phys 40:818

9 Babu SN, Hsu JH, Chen YS, and Lin JG (2010) J Appl Phys 107:09D919

10 Babu SN, Hsu JH, Chen YS, and Lin JG (2011) J Appl Phys 109:07D904